Original Article

BIO Integration

Targeted Imaging of Tumor Associated Macrophages in Breast Cancer

Yanni Xu[1,2,a], Yunting Zeng[1,2,a], Xiaoyun Xiao[1,a], Hejun Liu[3], Boyang Zhou[1,2], Baoming Luo[1], Phei Er Saw[2,*] and Qiongchao Jiang[1,2,*]

Abstract

Breast cancer is a highly heterogeneous disease lacking prognostic markers. Tumor-associated macrophages (TAMs) in the tumor microenvironment are associated with distant metastasis as well as poorer outcomes in breast cancer. Therefore, monitoring TAMs may guide prognostic assessment. This study explores an imaging modality based on a two-step click chemistry procedure for detecting TAMs in breast cancer. Mannose-targeted liposomes (MAN-lipo-AAG) and non-targeted liposomes (lipo-AAG) encapsulating Ac4GalNAz were prepared and comprehensively characterized. The sizes of the prepared MAN-lipo-AAG and lipo-AAG were 126 ± 0.22 and 93 ± 0.23 nm, respectively. *In vitro* studies demonstrated higher uptake of MAN-lipo-AAG than lipo-AAG by RAW264.7 cells. Moreover, flow cytometry and confocal microscopy confirmed that bright, homogeneous fluorescence labeling was present on RAW264.7 cell membranes in the MAN-lipo-AAG group. Furthermore, *in vivo* analysis indicated that MAN-lipo-AAG, compared with lipo-AAG, had higher accumulation in a 4T1 xenograft model and higher uptake by mannose-overexpressing TAMs. This study describes a promising approach for specific and non-invasive TAM-targeted imaging *via* metabolic glycoengineering.

Keywords

Breast cancer, CD206, click chemistry, tumor associated macrophages.

[1]Department of Ultrasound, Sun Yat-sen Memorial Hospital, Sun Yat-sen University, 107 Yanjiangxi Rd., Guangzhou 510120, China

[2]Guangdong Provincial Key Laboratory of Malignant Tumor Epigenetics and Gene Regulation, Sun Yat-sen Memorial Hospital, Sun Yat-sen University, Guangzhou 510120, China

[3]Department of Hyperbaric Oxygen, Sun Yat-sen Memorial Hospital, Sun Yat-sen University, 107 Yanjiangxi Rd., Guangzhou 510120, China

[a]These authors contributed equally to this work.
*Correspondence to: Qiongchao Jiang, E-mail: jiangqch3@mail.sysu.edu.cn; Phei Er Saw, E-mail: caipeie@mail.sysu.edu.cn

Received: March 18 2022
Revised: May 9 2022
Accepted: September 19 2022
Published Online: October 5 2022

Available at: https://bio-integration.org/

Introduction

An estimate of cancer-survivor prevalence has indicated that breast cancer is the most prevalent cancer among women [1]. Tumor-associated macrophages (TAMs), the major non-neoplastic constituent of the tumor microenvironment, are classified into two polarized types: M1, the antitumorigenic phenotype, and M2, the protumorigenic phenotype [2]. M2 TAMs tend to gather at the invasive tumor edge and hypoxic regions [3–5], and to exhibit numerous tumor-promoting properties, such as dampening antitumor immune responses, promoting angiogenesis, and matrix remodeling. Moreover, TAMs are directly correlated with the progression and metastasis of most cancers [6–8]. Macrophage infiltration affects clinical prognosis in breast cancer [9]. Thus, non-invasive labeling and observation of TAMs may greatly contribute to understanding of aspects of the microenvironment related to prognosis. However, the identification of TAMs in clinical practice can be confirmed only by immunohistochemistry, flow cytometry, or gene expression analyses, which are performed *in vitro*. Therefore, TAM-based molecular imaging *in vivo* has the potential to increase the feasibility of molecular classification, patient stratification, and prognostication of breast cancer in clinical settings.

In the past few years, interest has grown in developing imaging probes to monitor complex TAM responses. An ideal targeted reagent for molecular imaging should be highly expressed in targeted cells and should have a high-affinity binder to identify the molecule. The macrophage mannose receptor CD206, a classical M2-type macrophage marker, is highly expressed and widely used in targeted molecular techniques [10]. The characteristics of CD206 make it a promising target to assess the temporal and spatial localization of TAMs in the tumor microenvironment.

Recently, a click-mediated cell imaging strategy *via* metabolic labeling has been proposed as a promising novel approach to advance current molecular imaging methods [11, 12]. This strategy involves the generation of artificial receptors on specific cell types through metabolic engineering. Examples of unnatural glycan analogs for labeling include peracetylated

BIOI 2023, Vol 4, No. 3, 114–124
https://bio-integration.org doi: 10.15212/bioi-2022-0010

N-azidoacetylmannosamine (Ac4ManNAz, AAM) and peracetylated N-azidoacetylgalacto-samine (Ac4GalNAz, AAG), which are metabolized to N-acetylglucosamine or N-acetylgalactosamine, respectively. Through use of metabolic engineering to produce artificial receptors, sugars with chemical modifications are taken up by cells and can be used for the biosynthesis of cell-membrane-anchored salicylates [13]. However, the application of imaging glycans by metabolic labeling and bio-orthogonal click chemistry is limited by several factors including the absence of selectivity for cell types; thus, the azido-sugars can be taken up, transported, and metabolized by multiple cell types from different tissues after intravenous injection.

Herein, azido-sugars were encapsulated in mannose-targeted liposomes to increase their cell-type selectivity. Azido-sugars, as the potential imaging agent, were packaged in mannose/CD206 targeted liposomes (MAN-lipo-AAG) through a previously developed procedure. As shown in **Scheme 1**, MAN-lipo-AAG showed a near-spherical shape with a phospholipid bilayer structure with a diameter of ~126 nm. Owing to their self-enclosed structures, liposomes can entrap hydrophobic agents within the lipid bilayer. Furthermore, they protect loaded drugs, thus avoiding both degradation and undesirable effects of exposure to the environment on drug activity. The liposome surface was PEGylated through use of a liposomal formulation made of phosphatidylcholine, cholesterol, and DSPE-PEG2000-mannose. PEGylation sterically stabilizes liposomes and prolongs the liposome half-life in circulation, thus facilitating tumor uptake and accumulation. Mannose-modified liposomes also specifically target mannose receptors on TAMs, thus enhancing TAM-mediated tumor imaging. We hypothesized that liposomes encapsulating AAG would cross the reticuloendothelial system and thus enable metabolic labeling of sialoglycans on breast cancer cells with azides. MAN-lipo-AAG would then bind mannose/CD206-overexpressing TAMs and enter cells *via* endocytosis. The released azido-sugars were metabolically labeled on the surfaces of TAMs, thus prolonging the retention of DBCO-Cy5 for visualization of TAMs in breast cancer (**Scheme 1**).

Materials and methods

Materials

Phosphatidylcholine and cholesterol were obtained from Avanti Polar Lipids, Inc. (Alabaster, AL, United States). DSPE-PEG2000-mannose, DSPE-PEG2000, and DBCO-Cy5 were purchased from Xi'an Ruixi Biological Technology Co. Ltd (Xi'an, China). AAG and AAM, phosphate-buffered saline (PBS), Dulbecco's modified Eagle's medium, and fetal bovine serum were obtained from Invitrogen (Massachusetts, USA). EDTA, penicillin, and streptomycin were purchased from Thermo Fisher Scientific (Massachusetts, USA). DiL, DiR, a bicinchoninic acid protein assay kit, bovine serum albumin, Tris-buffered saline and Tween 20, sodium dodecyl sulfate-polyacrylamide electrophoresis gels, 2-(4-amidinophenyl)-6-indolecarbamidine dihydrochloride (DAPI), and methyl thiazolyl tetrazolium (MTT) were purchased from Beyotime Institute of Biotechnology (Shanghai, China). Hoechst 33342 was purchased from Sigma-Aldrich (Missouri, USA). LysoTracker Green DND-26 was obtained from Yeasen Biotech Co., Ltd (Shanghai, China). OCT tissue compound was purchased from Sakura Finetek USA Inc. (California, USA). Other chemicals and reagents were of analytical grade. Fluorescein isothiocyanate-conjugated rat anti-mouse F4/80 (FITC-F4/80) was purchased from BioLegend (California, USA). Polycarbonate membranes were purchased from Whatman, GE Healthcare (Illinois, USA). Well plates and confocal dishes were purchased from Corning (New York, USA).

The BALB/c-derived 4T1 mammary cancer cell line, RAW264.7 mouse macrophage cell line, and HEK-293T cell line were obtained from the Shanghai Institute of Cell

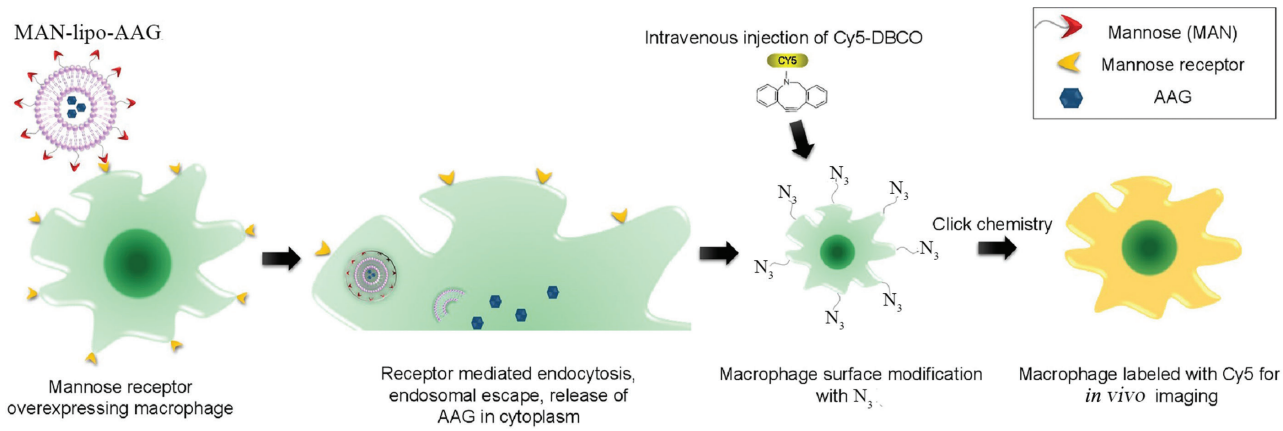

Scheme 1 Schematic illustration of tumor-associated macrophage (TAM)-targeted imaging through a two-step metabolic labeling and click reaction. The strategy was aimed at developing a diagnostic tool for the precise identification and imaging of TAMs in breast cancer. The azido-sugar AAG is first packaged in CD206 (mannose)-targeted liposomes (MAN-lipo-AAG). After systemic injection, MAN-lipo-AAG reaches the tumor site, owing to the enhanced permeation and retention (EPR) effect, and selectively binds TAMs. After receptor-mediated endocytosis, AAG is released into the cytoplasm and is metabolically converted to N-azidoacetylgalactosamine (GalNAz), which tags mucin-type O-linked glycans. The glycans are presented on the cell surfaces of TAMs. The azide groups of GalNAz then bind DBCO-Cy5, thus enabling *in vivo* imaging and identification of breast cancer.

Biology, Chinese Academy of Sciences. Female BALB/c mice, 6 weeks of age and weighing approximately 20 g, were purchased from Hunan SLAC Laboratory Animal Co. Ltd.

M2 phenotype macrophages abundant in breast cancer

Breast cancer cohort data for 1098 patients in the Cancer Genome Atlas (TCGA) were retrieved from UCSC Xena. As previously reported, the CIBERSORT (https://cibersort.stanford.edu/index.php) algorithm was used to transform normalized gene expression profiles obtained from TCGA into relative proportions of various types of immune cells in invasive breast carcinoma [14]. Samples with P values < 0.05 were included in further studies with application of the deconvolution algorithm. Prognostic analyses were conducted with Kaplan-Meier survival analysis.

Cell lines

The 4T1, RAW264.7, and HEK-293T cell lines were cultured in Dulbecco's modified Eagle's medium supplemented with 10% heat-inactivated fetal bovine serum, and 1% penicillin/streptomycin under 5% carbon-dioxide at 37°C. The 4T1 and HEK-293T cell lines were harvested with 0.25% EDTA, and RAW264.7 cells were harvested with cold PBS.

Animals

All research involving animals followed the Guide for the Care and Use of Laboratory Animals issued by the National Institutes of Health. Protocols in the study were authorized by the Committee on the Ethics of Animal Experiments, South China University of Technology.

Patients and tissue samples

Tumor tissues from 13 patients with breast cancer were obtained from Sun Yat-sen Memorial Hospital. Informed consent from relevant individuals and permission from the internal review board were obtained before collection of all samples (approval number: 2021-KY-046).

Establishment of 4T1 orthotopic models

A 50 μL volume of 4T1 cell suspension, containing 5×10^5 cells, was inoculated into the mammary fat pads of female mice and monitored daily. Experiments concluded when the mean diameters of the tumors reached approximately 40 mm^3.

Expression of CD206 in human breast cancer

M2 macrophage distribution was assessed through immunohistochemistry. Sections (4 μm) of human breast cancer tissue were cut for further staining. For CD206 staining, paraffin was first removed from samples with a xylene gradient, and samples were dehydrated with an ethanol gradient. Subsequently, 3% hydrogen peroxide was used to remove endogenous peroxidase. The samples were incubated with anti-mannose receptor antibody conjugated to horseradish-peroxidase (anti-CD206, ab64693, 1:100 dilution, Abcam, USA). Subsequently, DAB and hematoxylin staining were performed, and images were taken with a light microscope (ECLIPSE 80i, Nikon, Japan).

Preparation of azido-sugar-encapsulated liposomes

To determine the use of optimized azido-sugar, we first prepared liposomes encapsulating either AAG (MAN-lipo-AAG) or AAM (MAN-lipo-AAM). Both liposomes were composed of phosphatidylcholine cholesterol and DSPE-PEG2000-mannose in a 20:8:1 molar ratio in chloroform containing 12.9 mg of either AAG or AAM [15].

For non-targeted liposomes (lipo-AAG), the same molar mass of DSPE-PEG2000 was substituted for the ligand-containing lipids. The liposomes were obtained through the film hydration and extrusion method, in which lipids were dissolved in chloroform, blended well, and dehydrated into a lipid film before overnight vacuum disposal, as previously described [16]. To determine the cellular uptake and *in vivo* distribution of the liposomes, we prepared liposomes labeled with DiL (excitation wavelength/emission wavelength: 549/565 nm) and DiR (excitation wavelength/emission wavelength: 750/780 nm) (at 1 mol% of fluorophore). After sonication for 5–10 min, the acquired liposomes were extruded with a hand-held extruder, and 200 nm polycarbonate membranes were used to obtain highly homogeneous MAN-lipo-AAG and lipo-AAG.

Characterization of liposomes

The size distribution and zeta potential of MAN-lipo-AAG and lipo-AAG were evaluated with dynamic light scattering on a Zetasizer Nano ZS instrument (Malvern Instruments, Worcestershire, U.K.). MAN-lipo-AAG were diluted in PBS (final concentration at 0.1 mg/mL) for transmission electron microscopy (TEM, 7700 electron microscope, HITACHI) imaging. The concentrations of encapsulated AAG were assessed with reverse-phase high-performance liquid chromatography (HPLC) after complete lysis of liposomes with acetonitrile [17]. Analytical HPLC was performed on an Agilent 1260 Infinity Quaternary HPLC System equipped with a VWD UV-visible detector, and a ZORBAX Eclipse XDB-C18 column. AAG stock solution was added separately to 200 μL blank acetonitrile to obtain AAG concentrations of 1, 0.5, 0.25, 0.125, and 0.625 mg/mL. AAG quality-control samples were analyzed with HPLC. The standard curves between the peak areas of AAG in quality control samples and AAG concentration were evaluated with least-squares regression analysis. The

standard curve was linear ($r^2 = 0.1$) over the range 0.625–1 mg/mL in acetonitrile.

Cell-surface azide-group labeling

RAW264.7 cells seeded in six-well plates at a concentration of 2×10^5 cells/mL were cultured overnight before incubation with AAG and MAN-lipo-AAG at 37°C for 24 h. Subsequently, cells were incubated with DBCO-Cy5 at a final concentration was 20 μM for 30 min, for flow cytometry (Accuri C6; BD Biosciences), western blot analysis, or fluorescence microscopy analysis [18–20].

For flow cytometry analysis, 10^4 cells per test were analyzed in FlowJo software (TreeStar, San Carlos).

For western blot assays, RAW264.7 cells were harvested, and lysates were extracted directly without incubation with DBCO-Cy5; the lysates were then subjected to biotinylation *via* co-incubation with DBCO-PEG4-biotin and were reacted with streptavidin-horseradish peroxidase conjugate. The concentrations of extracted proteins were evaluated with bicinchoninic acid assays. Proteins were loaded onto 10% sodium dodecyl sulfate-polyacrylamide electrophoresis gels after denaturation at 95°C. Samples were transferred to a Hybond P membrane, which was blocked with 5% bovine serum albumin in Tris-buffered saline and Tween 20 for 1 h, and developed with a western blotting system.

For fluorescence microscopy analysis, cells were fixed for 15 min in paraformaldehyde at room temperature and stained with DAPI to label nuclei. All images were acquired through confocal laser scanning microscopy (CLSM, Zeiss LSM 710, Germany).

Liposome intracellular tracking

Cells were seeded onto confocal dishes at a concentration of 1×10^5 cells. After 24 h, the cells were incubated with DiL-labeled lipo-AAG and MAN-lipo-AAG liposomes at 37°C for 30 min, then incubated with 5 μg/mL Hoechst 33342 and LysoTracker Green DND-26 for 15 min at 37°C. Images were taken under CLSM (Zeiss LSM 710, Germany).

Cell viability experiments

To evaluate cell viability, we incubated RAW264.7 and HEK-293T cells seeded at 1×10^4 cells per well on 96-well plates with sequential concentrations (12.5, 25, 50, 75, and 100 μM) of MAN-lipo-AAG and Lipo-AAG for 24 h before incubation with MTT solution (20 μL per well, 5 mg/mL) for 4 h. The culture medium was then switched to 150 μL dimethyl sulfoxide. After 10 min, the absorbance at 490 nm was detected with a microplate reader (BioTek).

Liposome biodistribution

To investigate the *in vivo* biodistribution of liposomes, we injected DiR labeled MAN-lipo-AAG and lipo-AAG (administered lipid equivalent to 50 mg/kg AAG per mouse) into 4T1 tumor-bearing BALB/c mice through the tail vein. Mice (n = 3 per group) were imaged 24 h after injection with an *in vivo* fluorescence (NIRF) imaging system (Bruker). The major organs and tumors of each sacrificed mouse were collected for *ex vivo* NIRF imaging.

NIRF imaging of macrophages

For *in vivo* macrophage-targeted NIRF imaging, PBS (negative control), free AAG, lipo-AAG, or MAN-lipo-AAG was administered intravenously (*i.v.*) once per day to each 4T1-tumor-bearing mouse for three consecutive days (administered lipid equivalent to 50 mg/kg AAG per mouse). DBCO-Cy5 (5 mg/kg) was *i.v.* injected on the fourth day. At 24 h after DBCO-Cy5 injection, mice (n = 3 per group) were imaged with the NIRF imaging system (Bruker).

Immunofluorescence staining

For *ex vivo* NIRF imaging, the tumors from the mice were harvested after *in vivo* macrophage-targeted NIRF imaging. The tumors were placed in 4% paraformaldehyde solution for fixation and implanted in OCT tissue compound on dry ice, and complete transverse slices of 8 μm were obtained. For staining of macrophages, frozen tissue sections of breast tumor xenografts stained with FITC-F4/80 and then counter-stained with DAPI were subjected to fluorescence imaging with an Olympus BX63 microscope.

Statistical analysis

Quantitative data analyzed in GraphPad Prism (version 5.0) are shown as mean ± SD. Statistical significance, defined as P values < 0.05, was assessed with one-way ANOVA and unpaired Student's t-test.

Results

Distribution of TAMs in breast cancer

We first performed immunohistochemical analysis to assess the TAM expression in samples from 13 patients with breast cancer. As shown in **Figure 1A**, TAMs appeared to be more localized near the tumor margin than the tumor core. We also performed immunofluorescence analysis to assess the distribution of macrophages in 4T1 tumor models. As indicated in **Figure 1B**, CD206 staining localized near the tumor margin, similarly to the clinical presentation of patients with breast cancer. To assess the importance of TAMs in breast cancer, the abundance of TAMs in patients with breast cancer was obtained from TCGA database, and their RNA-seq data were analyzed with CIBERSORT. As indicated in **Figure 1C**, survival analysis showed that a high abundance of TAMs

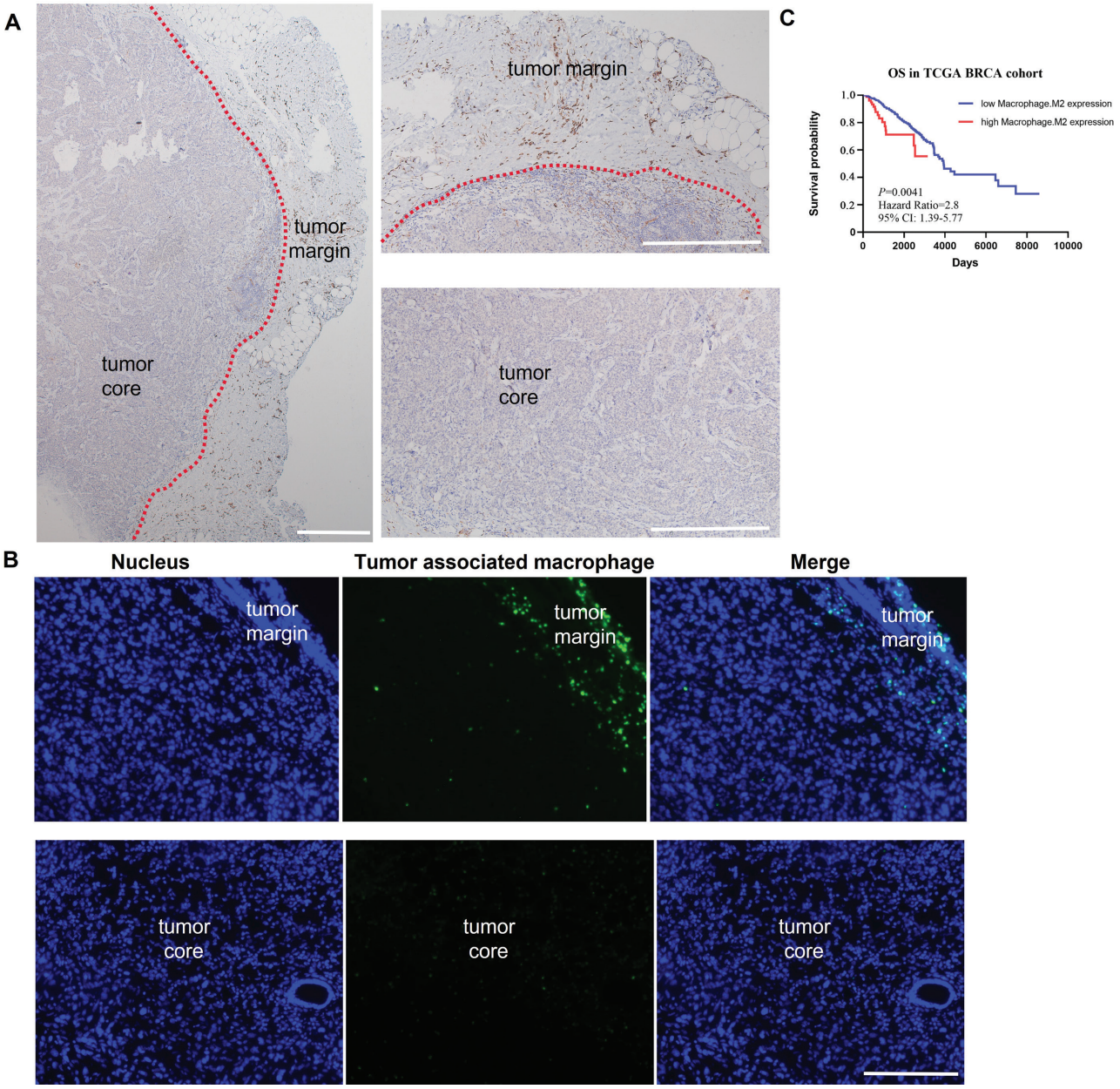

Figure 1 A. CD206 expression on macrophages in human breast cancer, observed by immunohistochemistry. Higher intensity was detected at the breast cancer boundary, and lower density was detected at the tumor core. B. Distribution of TAMs in 4T1 xenograft models, demonstrated by fluorescence immunoassays. Higher fluorescence intensity was detected at the tumor margin, and lower intensity was detected at the tumor core. C. M2 TAMs correlated with overall survival in breast cancer, on the basis of data from TCGA database. Scale bar = 250 μm.

was associated with poor overall survival in patients with breast cancer (hazard ratio = 2.8, 95% CI (confidence interval) = 1.39–5.77, P = 0.0041). Therefore, increased TAMs appeared to predict poor outcomes in breast cancer.

Selectivity of azido-sugars

We first explored the metabolic-labeling effects of AAM or AAG in macrophage-like RAW264.7 cells *in vitro*. RAW264.7 cells were incubated with a previously optimized concentration of AAM or AAG (20 μM, 50 μM, or 75 μM) for 24 h. The azido groups generated on the cell surface were tested by fluorescence microscopy and western blot analysis. Fluorescence microscopy analysis indicated that RAW264.7 cells had substantially stronger fluorescence signals after treatment with AAG than AAM (**Figure 2A**), and the fluorescence intensity was directly proportional to the concentration of the azido-sugars. In western blot assays, RAW264.7 were harvested, and extracted lysate samples were biotinylated by co-incubation with DBCO-PEG4-biotin, then reacted with streptavidin-horseradish peroxidase conjugate. The results indicated stronger intensity of DBCO-PEG4-biotin bound to RAW264.7 macrophages incubated with AAG than AAM (**Figure 2B**), thus demonstrating AAG's better suitability for subsequent experiments. The presence of the azide groups decreased at a concentration of 75 μM AAG, probably because of its cell toxicity. In subsequent experiments, 50 μM AAG was chosen as the optimal concentration because it had the

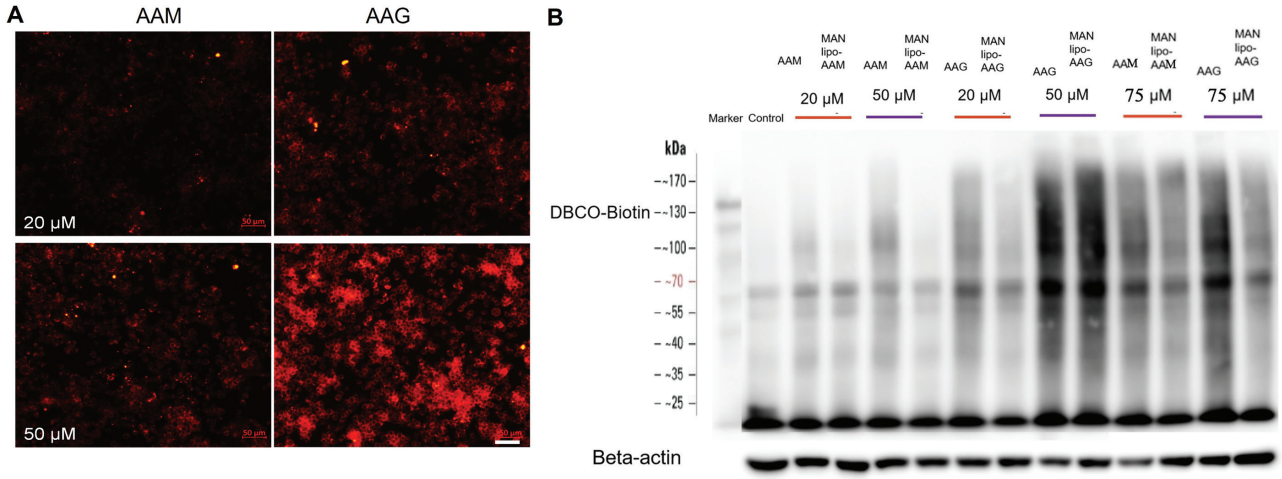

Figure 2 A. Fluorescence microscopy analysis indicating substantially stronger fluorescence signals of RAW264.7 cells in the presence of AAG rather than AAM. B. Western blot analysis indicating the generation of the largest amounts of azide groups in RAW264.7 cell lysate with 50 μM AAG treatment. Scale bar = 50 μm.

highest presence of azide groups among the 20, 50, and 75 μM concentrations.

Preparation of CD206-targeted liposomes encapsulating azido-sugars

To develop high-functionality mannose-receptor-over-expressing macrophage-targeted liposomes, we prepared CD206-targeted liposomes (MAN-lipo-AAG). To determine the loading of encapsulated AAG in MAN-lipo-AGG, we diluted prepared liposome solution with acetonitrile-water solution (1:1, v/v) to a final concentration of 10% (v/v). HPLC measurements were conducted to determine the amount of encapsulated AAG in the prepared liposomes, according to a standard curve (**Figure 3A, B**). Comparison of the peak area of our sample (60.06) against the standard curve indicated an AAG concentration of 0.267 mg/mL in the MAN-lipo-AAG sample. The HPLC results indicated that MAN-lipo-AAG had an encapsulation efficiency of AAG at 89% (encapsulation efficiency = final concentration/initial concentration = 0.267/0.3 mg/mL). Dynamic light scattering analysis demonstrated that the average hydrodynamic size of lipo-AAG and MAN-lipo-AAG was 93 ± 0.23 nm and 126 ± 0.22 nm, respectively. Zeta potential values indicated that lipo-AAG had a charge of 0.32 ± 0.01 mV, and MAN-lipo-AAG had a charge of 1.13 ± 0.02 mV; these values were significantly different. The zeta-potential of MAN-lipo-AAG was slightly higher than that of lipo-AAG, owing to the fewer methoxy groups in the DSPE-PEG2000 component of lipo-AAG, thus potentially facilitating greater liposome uptake by cells *via* interaction with the cell membrane through electrostatic interactions with negatively charged phospholipids or membrane proteins. The physical characteristics of lipo-AAG and MAN-lipo-AAG are summarized in **Figure 3C**. TEM images (**Figure 3D**) also indicated that MAN-lipo-AAG had the same morphology, comprising a spherical structure with a diameter of approximately 120 nm.

Ideally, the approach of macrophage labeling and tracking should be non-cytotoxic and should have minimal effects on the functions of cell lines. Therefore, we confirmed the toxicity of AAG and this liposomal system in RAW264.7 macrophages and HEK-293T cells. The cytotoxicity of MAN-lipo-AAG, lipo-AAG, and PBS (control) was evaluated at five increasing concentrations of AAG (12.5, 25, 50, 75, or 100 μM) for 24 h. As shown in **Figure 3E**, RAW264.7 macrophages or HEK-293T cells incubated with lipo-AAG or MAN-lipo-AAG at concentrations below 75 μM showed no significant changes in cell viability; approximately 80% and 90% viability, respectively, was observed after 50 μM treatment for 24 h, thus indicating minimal cytotoxicity with good biocompatibility.

Cellular uptake of liposomes

To confirm whether MAN-lipo-AAG enters cells *via* receptor-assisted endocytosis, we first encapsulated 50 μM MAN-lipo-AAG or lipo-AAG with DiL to verify their co-localization with lysosomes. As indicated in **Figure 4A**, MAN-lipo-AAG were effectively internalized into endosomes through CD206-mediated endocytosis. In contrast, MAN-lipo-AAG showed minimal binding to CD206-negative 4T1 cells, and subsequently showed little translocation to lysosomes. For lipo-AAG, similar minimal binding to both RAW264.7 macrophages and 4T1 cells was observed, thus indicating that mannose (CD206) recognition was essential for receptor-mediated liposome uptake.

Generation of azido-sugars on the surfaces of macrophages

To demonstrate whether MAN-lipo-AAG could transport sufficient unnatural sugars into the cytosol and incorporate AAG into sialyglycoproteins, we treated RAW264.7 cells

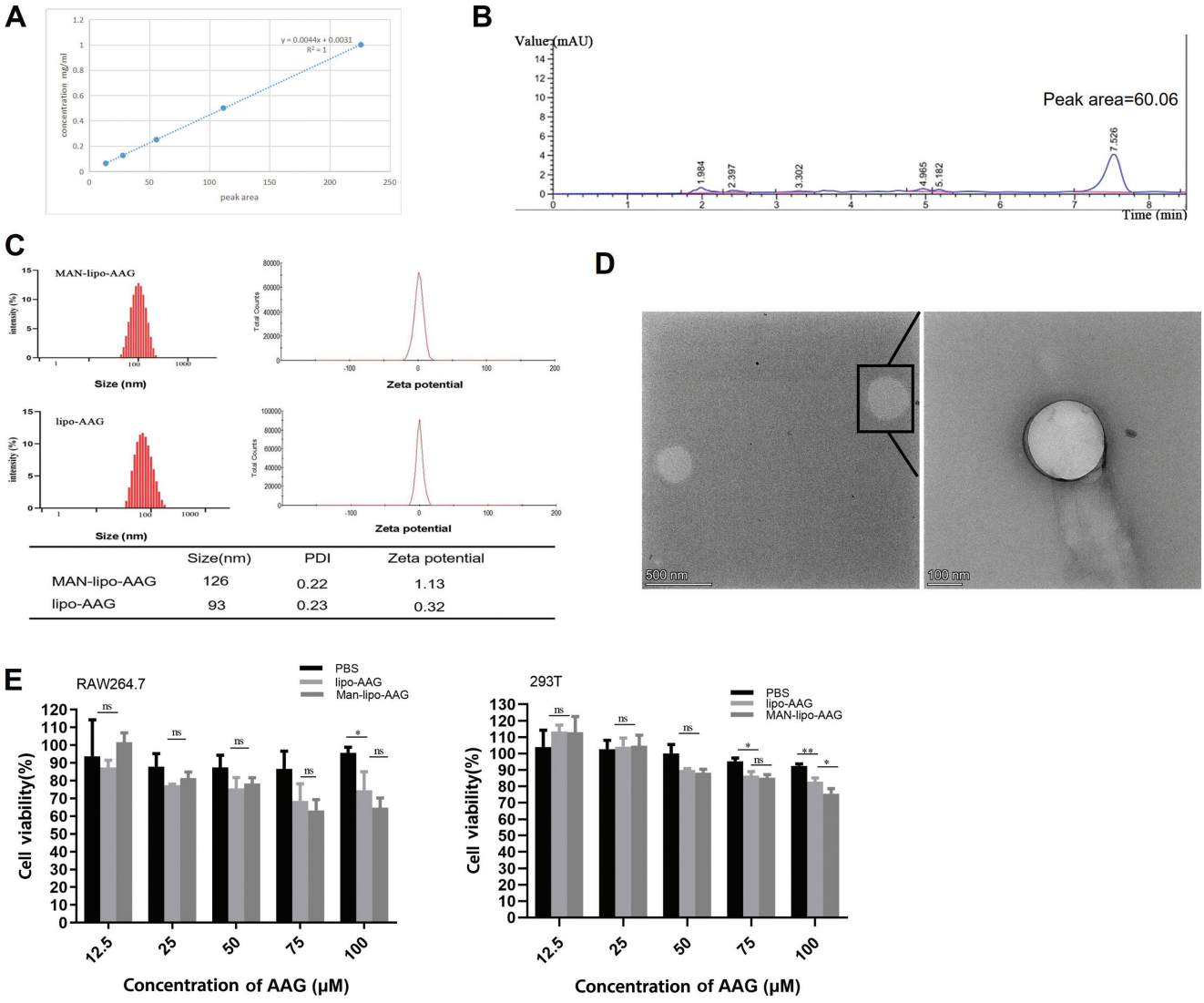

Figure 3 A. The standard curve was linear (r^2 = 0.1) over the range 0.625–1 mg/mL in acetonitrile. B. Quantification of AAG encapsulation efficiency *via* HPLC analysis: the peak area of AAG from MAN-lipo-AAG was 60.06. C. Diameter distribution and zeta potential of lipo-AAG and MAN-lipo-AAG. D. TEM images of MAN-lipo-AAG, indicating a spherical structure with a diameter of approximately 120 nm. E. Cell viability test for PBS, lipo-AAG, and MAN-lipo-AAG, determined with MTT assays. RAW264.7 macrophages and HEK-293T cells incubated with lipo-AAG and MAN-lipo-AAG showed no significant changes in cell viability at liposome concentrations lower than 75 μM, and showed approximately 80% and 90% viability, respectively after treatment with 50 μM liposomes for 24 h, thus indicating minimal cytotoxicity with good biocompatibility. **P*<0.05; ***P*<0.01; ns: no significance.

with PBS, free AAG, or MAN-lipo-AAG for 24 h, then performed 20 μM DBCO-Cy5 labeling, and further analysis with flow cytometry and CLSM. The robust fluorescence labeling observed in the MAN-lipo-AAG group was comparable to that in AAG-treated cells, thus indicating that a similar amount of AAG was present in the cells in both groups (**Figure 4B, C**). Subsequent CLSM analysis indicated that AAG was present mainly on the cell membrane (**Figure 4D**), thus indicating that the azido-sugar was generated on RAW264.7 cells.

Tumoral uptake and biodistribution of MAN-lipo-AAG *in vivo*

Inspired by the *in vitro* data, we analyzed the properties of MAN-lipo-AAG in 4T1 tumor-bearing BALB/c mice to target *in vivo* tumors. For *in vivo* imaging, we used DiR fluorophore-labeled MAN-lipo-AAG and lipo-AAG. Both MAN-lipo-AAG and lipo-AAG were injected through the tail vein (*i.v.*) into mice (n = 3 per group). As shown in **Figure 5A** at 24 h, tumors of mice treated with MAN-lipo-AAG had a fluorescence intensity of approximately 121 AU, indicating a six-fold increase in fluorescence intensity with respect to the 18 AU observed in the lipo-AAG treated mice (**Figure 5C**). MAN-lipo-AAG also showed significantly higher tumor uptake and a longer tumor residence time than lipo-AAG.

To determine the biodistribution of MAN-lipo-AAG and lipo-AAG, we euthanized mice after imaging. The tumor and major organs (inclusive of heart, liver, kidney, lung, and spleen) were subjected to NIRF imaging. As shown in **Figure 5B**, the tumoral uptake of MAN-lipo-AAG was higher than those in the PBS negative control and lipo-AAG groups. Interestingly, the MAN-lipo-AAG group showed lower uptake in other major organs, thus indicating that

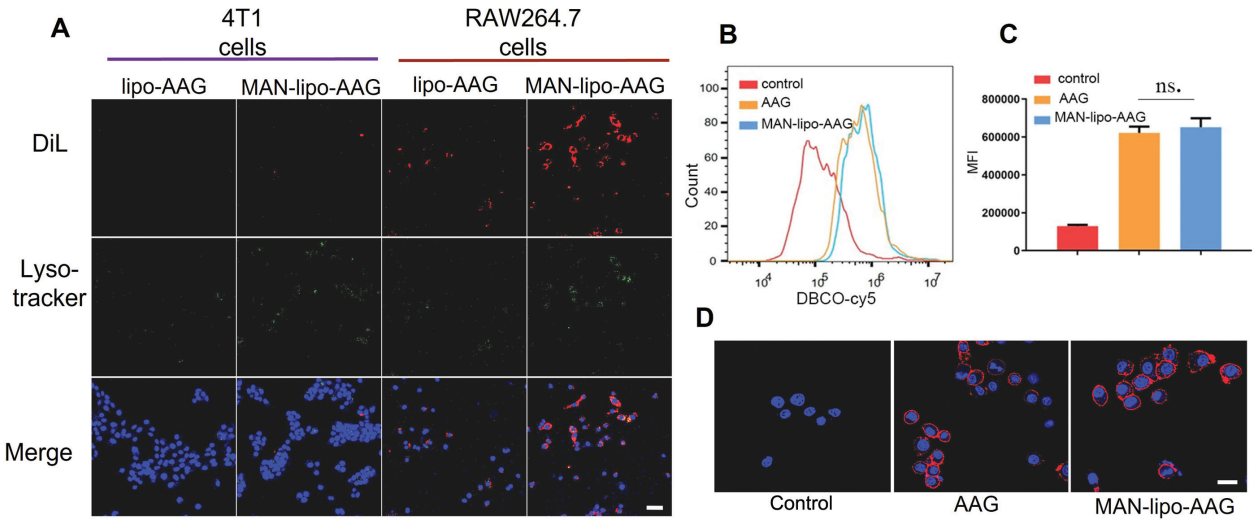

Figure 4 A. CLSM images of cellular uptake and subcellular localization. 4T1 and RAW 264.7 cells were treated with lipo-AAG or MAN-lipo-AAG for 30 min at 37°C. Scale bar = 50 μm. B, C. Flow cytometry analysis of azido-sugar generation on the surfaces of RAW 264.7 cells treated with PBS (control), free AAG, or MAN-lipo-AAG for 24 h, and stained with DBCO-Cy5 for 24 h (ns: no significance). D. CLSM images of azido-sugar generation on the surfaces of RAW 264.7 cells treated with PBS (control), free AAG, or MAN-lipo-AAG for 24 h, and stained with DBCO-Cy5 for 24 h. Scale bar = 20 μm.

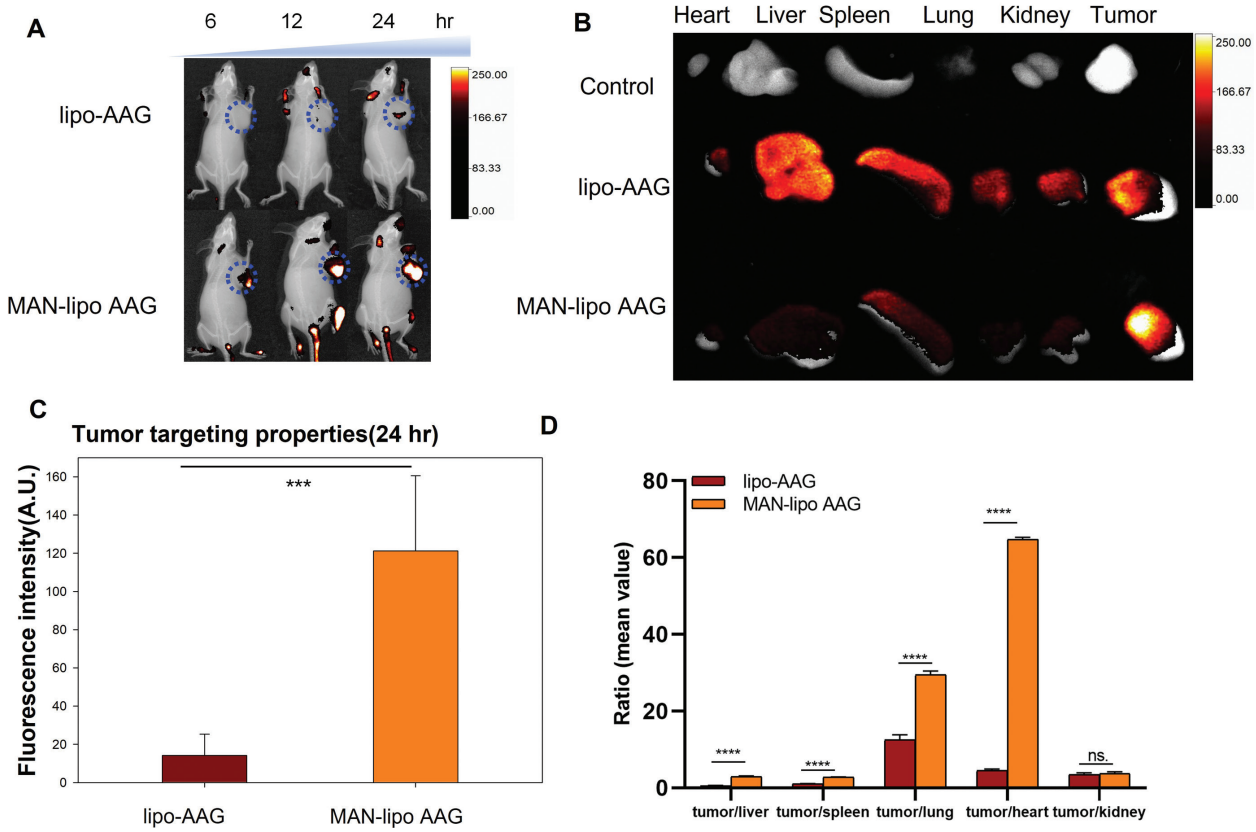

Figure 5 A. Fluorescence imaging indicating the biodistribution of lipo-AAG and MAN-lipo-AAG *in vivo*. B. Representative *ex vivo* fluorescence imaging of mouse organs with different treatments. C, D. Fluorescence intensities of the tumors and major organs (abscissa displays the ratio of tumor fluorescence to that of other organs). The results are expressed as mean ± S. D. (n = 3; ***P<0.001; ****P<0.0001; ns: no significance).

MAN-lipo-AAG selectively accumulated in tumors and demonstrated lower non-selective uptake in other organs (**Figure 5B, D**).

In vivo fluorescence imaging of CD206 macrophages after AAG labeling *via* click chemistry

We then examined the selective labeling efficacy of MAN-lipo-AAG *via* click chemistry *in vivo*. Mice (n = 12) were treated with PBS, free AAG, lipo-AAG, or MAN-lipo-AAG. After 24 h, DBCO-Cy5 (5 mg/kg) was *i.v.* injected. NIRF whole body images were monitored with *in vivo* fluorescence imaging. As shown in **Figure 6A**, Cy5 fluorescence was detected at different intensities in all groups (free AAG, lipo-AAG, and MAN-lipo-AAG groups). Among them, the MAN-lipo-AAG-treated group demonstrated significantly greater Cy5 fluorescence intensity in tumor tissue than the other groups, thus indicating the targeting ability of MAN-lipo-AAG *in vivo*.

To identify the co-localization of TAMs and DBCO-Cy5, we performed immunofluorescence analysis. The Cy5 fluorescence of all three groups was markedly higher than that in the control group (**Figure 6B**, $P < 0.001$). In the MAN-lipo-AAG group, Cy5 fluorescence merged

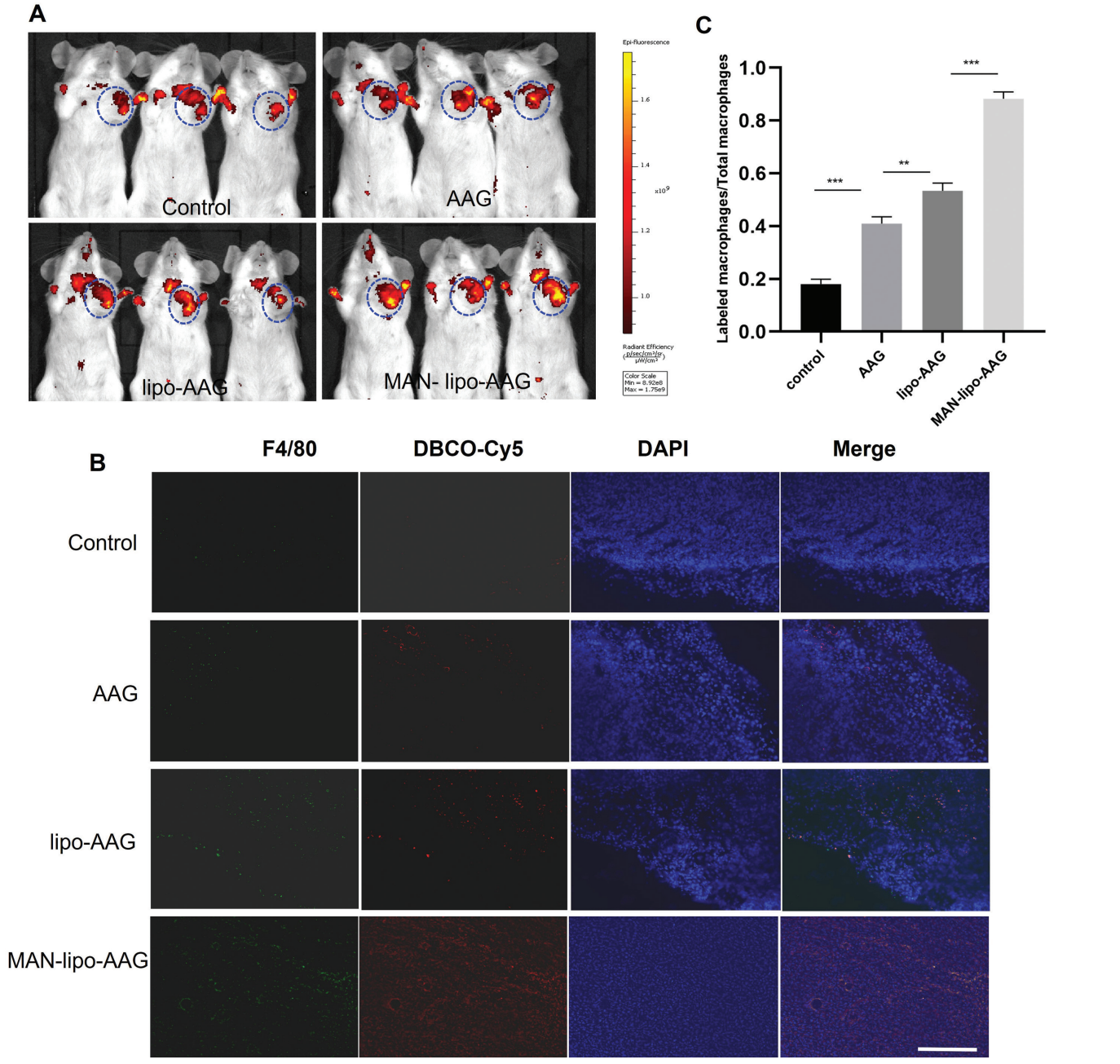

Figure 6 *In vivo* assessment of the MAN-lipo-AAG-based two-step tumor-targeting strategy. A. *In vivo* whole-body fluorescence imaging of BALB/c mice pretreated with PBS, free AAG, lipo-AAG, or MAN-lipo-AAG, followed by DBCO-Cy5 injection after 24 h. B. Immunofluorescence analysis of the co-localization of macrophages and DBCO-Cy5. Scale bar = 250 μm. C. Significantly enhanced fluorescence in all three groups compared with the control. In the MAN-lipo-AAG group, Cy5 fluorescence merged perfectly with FITC-labeled F4/80 staining of macrophages, and only minimal Cy5 fluorescence was detected in the lipo-AAG group (**P<0.01; ***P<0.001).

perfectly with macrophages, whereas only minimal Cy5 fluorescence was detected in the lipo-AAG group (**Figure 6C**), thus indicating that MAN-lipo-AAG labeled TAMs with azido groups and were stained with DBCO-Cy5 *via* click reactions.

Discussion

Development of diagnostic methods and effective treatments is urgently needed because of breast cancer's increasing incidence and fatality rates over the past few decades. Our study revealed that high TAM expression was associated with shorter overall survival of patients with breast cancer. Interestingly, TAMs were observed at the tumor edge (rather than the tumor core) in a 4T1 xenograft tumor model and in patients with breast cancer, thus indicating the importance of TAM-targeted imaging and its potential ability to monitor tumor size. Herein, we developed azido-sugar-encapsulated CD206-targeted liposomes that can be used for the detection of TAMs.

In this study, we exploited the ability of AAG to metabolically label TAMs with chemical reporters by using CD206-targeted liposomes. With cell-specific or tissue-specific promoters, most genetically encoded protein tags can be readily contained within specific types of cells. High expression of CD206 in TAMs has been verified by previous studies [21] and may serve as a potential candidate detection target [22, 23]. However, conventional tumor-targeting strategies have several limitations. First, the unstable antigenic profiles of cancer cells hinder accurate and efficient cell tracking. Second, antibodies display poor penetration in solid tumors. In addition, antibody-based imaging is characterized by low labeling efficiency and by signal dilution. Interestingly, in contrast to proteins, glycans are difficult to label in a cell-specific manner. However, click chemistry, a strategy based on the introduction of chemical groups such as azido groups onto the extracellular surface [17, 24], can achieve high efficiency and reaction yields, and simulate the function of receptors on cell membranes.

Using CD206-targeted liposomes, we found that the delivered azido-sugars produced azido groups on the surfaces of macrophages with high CD206 expression but not 4T1 cells with minimal CD206 expression *in vitro* and *in vivo*. A two-step reaction cascade of click chemistry was used to first artificially express azido-sugars selectively on the targeted cell surface, and then to introduce fluorophore-conjugated DBCO, which binds only these expressed azido-sugars, thus facilitating selective targeting. Furthermore, the *in vivo* biodistribution of MAN-lipo-AAG indicated that CD206 targeting enriched the accumulation of MAN-lipo-AAG in TAMs, which were localized in tumor tissue. Internalization of these MAN-lipo-AAG then generated artificial azide groups that were used for imaging, thus supporting the use of CD206 as an indicator for TAM imaging. Moreover, MAN-lipo-AAG persisted in the bloodstream for 24 h, thus demonstrating the stability of this nanoplatform *in vivo*.

The 4T1 cell line shows growth characteristics highly similar to those of invasive human metastatic breast tumors [25] and is often applied in breast cancer research associated with TAMs [26, 27]. However, owing to the molecular heterogeneity of breast cancer, novel imaging agents should be used in models that better recapitulate human breast cancer, such as patient derived xenograft (PDX) models. PDXs generated from fresh tumor specimens faithfully reproduce human tumors, including the diversity of breast tumors, histopathology, tumor behavior, and metastatic properties. In the future studies, we plan to evaluate the efficacy of MAN-lipo-AAG in PDX models.

However, on the basis of our findings, this strategy has clear advantages over conventional labeling methods based on antibodies, because azido-sugars loaded in mannose-targeted liposomes make TAMs more targetable at a higher density than typical antigens, thus overcoming limitations such as low labeling efficiency and signal dilution, which encumber precise and efficient cell tracking. Hence, our strategy for TAM imaging offers a promising approach for basic and applied research on biomedical applications. Additionally, imaging and reprogramming of TAMs may be performed concurrently in the future.

Conclusion

Herein, we designed M2-macrophage-specific mannose-targeted liposomes (MAN-lipo-AAG) based on bio-orthogonal click-chemistry reactions. MAN-lipo-AAG boosted the targeting ability of the DBCO–Cy5 conjugate through a click reaction and specifically targeted CD206-overexpressing TAMs, thus supporting TAM-targeted imaging in breast cancer.

Acknowledgements

This study was supported by the National Natural Science Foundation of China (82001822, 81701715, and 81873899); and The Science Foundation of Guangdong Province (2017A030310200, 2018A030313097, and 2021A1515012611).

Abbreviations

TCGA:	The Cancer Genome Atlas
DSPE-PEG2000:	1,2-distearoyl-sn-glycero-3-phosphoethanolamine-N-methoxy (polyethylene glycol)-2000
DSPE-PEG2000-mannose:	1,2-distearoyl-sn-glycero-3-phosphoethanolamine-N-mannose (polyethylene glycol)-2000
AAG:	N-azidoacetylgalactosamine-acetylated, Ac4GalNAz
AAM:	N-azidoacetylmannosamine-tetraacylated, Ac4ManNAz
lipo-AAG:	non-targeted liposomes
MAN-lipo-AAG:	mannose-targeted liposomes
HPLC:	high-performance liquid chromatography
PBS:	phosphate-buffered saline

DiL:	1,1¢-dioctadecyl-3,3,3´,3´-tetramethylindocarbocyanine	MTT:	methyl thiazolyl tetrazolium
DiR:	1,1-dioctadecyl-3,3,3,3-tetramethylindotricarbocyaineiodide	DMSO:	dimethyl sulfoxide
DAPI:	2-(4-Amidinophenyl)-6-indolecarbamidine dihydrochloride	h:	hour
		min:	minute
		°C:	degrees centigrade
		μM:	μmol/L

References

[1] Siegel RL, Miller KD, Fuchs HE, Jemal A. Cancer statistics, 2021. CA: Cancer J Clin 2021;71:7-33. [PMID: 33433946 DOI: 10.3322/caac.21654]

[2] Mantovani A, Locati M. Tumor-associated macrophages as a paradigm of macrophage plasticity, diversity, and polarization: lessons and open questions. Arterioscler Thromb Vasc Biol 2013;33:1478-83. [PMID: 23766387 DOI: 10.1161/ATVBAHA.113.300168]

[3] Zheng X, Weigert A, Reu S, Guenther S, Mansouri S, et al. Spatial density and distribution of tumor-associated macrophages predict survival in non-small cell lung carcinoma. Cancer Res 2020;80:4414-25. [PMID: 32699134 DOI: 10.1158/0008-5472.CAN-20-0069]

[4] Baxevanis CN, Sofopoulos M, Fortis SP, Perez SA. The role of immune infiltrates as prognostic biomarkers in patients with breast cancer. Cancer Immunol Immunother 2019;68:1671-80. [PMID: 30905043 DOI: 10.1007/s00262-019-02327-7]

[5] Chaturvedi P, Gilkes DM, Takano N, Semenza GL. Hypoxia-inducible factor-dependent signaling between triple-negative breast cancer cells and mesenchymal stem cells promotes macrophage recruitment. Proc Natl Acad Sci U S A 2014;111:E2120-9. [PMID: 24799675 DOI: 10.1073/pnas.1406655111]

[6] Spill F, Reynolds DS, Kamm RD, Zaman MH. Impact of the physical microenvironment on tumor progression and metastasis. Current opinion in biotechnology 2016;40:41-8. [PMID: 26938687 DOI: 10.1016/j.copbio.2016.02.007]

[7] Wu K, Lin K, Li X, Yuan X, Xu P, et al. Redefining tumor-associated macrophage subpopulations and functions in the tumor microenvironment. Front Immunol 2020;11:1731. [PMID: 32849616 DOI: 10.3389/fimmu.2020.01731]

[8] Yang M, Li Z, Ren M, Li S, Zhang L, et al. Stromal infiltration of tumor-associated macrophages conferring poor prognosis of patients with basal-like breast carcinoma. J Cancer 2018;9:2308-16. [PMID: 30026826 DOI: 10.7150/jca.25155]

[9] DeNardo DG, Brennan DJ, Rexhepaj E, Ruffell B, Shiao SL, et al. Leukocyte complexity predicts breast cancer survival and functionally regulates response to chemotherapy. Cancer Discov 2011;1:54-67. [PMID: 22039576 DOI: 10.1158/2159-8274.CD-10-0028]

[10] Cassetta L, Fragkogianni S, Sims AH, Swierczak A, Forrester LM, et al. Human tumor-associated macrophage and monocyte transcriptional landscapes reveal cancer-specific reprogramming, biomarkers, and therapeutic targets. Cancer Cell 2019;35:588-602.e10. [PMID: 30930117 DOI: 10.1016/j.ccell.2019.02.009]

[11] Taiariol L, Chaix C, Farre C, Moreau E. Click and bioorthogonal chemistry: the future of active targeting of nanoparticles for nanomedicines? Chem Rev 2022;122:340-384. [DOI: 10.1021/acs.chemrev.1c00484]

[12] Yoon HY, Koo H, Kim K, Kwon IC. Molecular imaging based on metabolic glycoengineering and bioorthogonal click chemistry. Biomaterials 2017;132:28-36. [PMID: 28399460 DOI: 10.1016/j.biomaterials.2017.04.003]

[13] Boyce M, Carrico IS, Ganguli AS, Yu SH, Hangauer MJ, et al. Metabolic cross-talk allows labeling of O-linked beta-N-acetylglucosamine-modified proteins via the N-acetylgalactosamine salvage pathway. Proc Natl Acad Sci U S A 2011;108:3141-6. [PMID: 21300897 DOI: 10.1073/pnas.1010045108]

[14] Newman AM, Liu CL, Green MR, Gentles AJ, Feng W, et al. Robust enumeration of cell subsets from tissue expression profiles. Nat Methods 2015;12:453-7. [PMID: 25822800 DOI: 10.1038/nmeth.3337]

[15] Shen L, Cai K, Yu J, Cheng J. Novel liposomal azido mannosamine lipids on metabolic cell labeling and imaging via Cu-Free click chemistry. Bioconjugate Chem 2019;30:2317-22. [DOI: 10.1021/acs.bioconjchem.9b00509]

[16] Jiang Q, Zeng Y, Xu Y, Xiao X, Liu H, et al. Ultrasound molecular imaging as a potential non-invasive diagnosis to detect the margin of hepatocarcinoma via CSF-1R targeting. Front Bioeng Biotechnol 2020;8:783. [PMID: 32760707 DOI: 10.3389/fbioe.2020.00783]

[17] Sun Y, Hong S, Xie R, Huang R, Lei R, et al. Mechanistic investigation and multiplexing of liposome-assisted metabolic glycan labeling. J Am Chem Soc 2018;140:3592-602. [DOI: 10.1021/jacs.7b10990]

[18] Sheta R, Woo CM, Roux-Dalvai F, Fournier F, Bourassa S, et al. A metabolic labeling approach for glycoproteomic analysis reveals altered glycoprotein expression upon GALNT3 knockdown in ovarian cancer cells. J Proteomics 2016;145:91-102. [PMID: 27095597 DOI: 10.1016/j.jprot.2016.04.009]

[19] Han SS, Lee DE, Shim HE, Lee S, Jung T, et al. Physiological effects of Ac4ManNAz and optimization of metabolic labeling for cell tracking. Theranostics 2017;7:1164-76. [PMID: 28435456 DOI: 10.7150/thno.17711]

[20] Mongis A, Piller F, Piller V. Coupling of immunostimulants to live cells through metabolic glycoengineering and bioorthogonal click chemistry. Bioconjugate Chem 2017;28:1151-65. [DOI: 10.1021/acs.bioconjchem.7b00042]

[21] Jaynes JM, Sable R, Ronzetti M, Bautista W, Knotts Z, et al. Mannose receptor (CD206) activation in tumor-associated macrophages enhances adaptive and innate antitumor immune responses. Sci Transl Med 2020;12:eaax6337. [PMID: 32051227 DOI: 10.1126/scitranslmed.aax6337]

[22] Movahedi K, Schoonooghe S, Laoui D, Houbracken I, Waelput W, et al. Nanobody-based targeting of the macrophage mannose receptor for effective in vivo imaging of tumor-associated macrophages. Cancer Res 2012;72:4165-77. [PMID: 22719068 DOI: 10.1158/0008-5472.CAN-11-2994]

[23] Locke LW, Mayo MW, Yoo AD, Williams MB, Berr SS. PET imaging of tumor associated macrophages using mannose coated 64Cu liposomes. Biomaterials 2012;33:7785-93. [PMID: 22840225 DOI: 10.1016/j.biomaterials.2012.07.022]

[24] Takayama Y, Kusamori K, Nishikawa M. Click chemistry as a tool for cell engineering and drug delivery. Molecules (Basel, Switzerland) 2019;24:172. [PMID: 30621193 DOI: 10.3390/molecules24010172]

[25] Guy CT, Cardiff RD, Muller WJ. Induction of mammary tumors by expression of polyomavirus middle T oncogene: a transgenic mouse model for metastatic disease. Mol Cell Biol 1992;12:954-61. [PMID: 1312220 DOI: 10.1128/mcb.12.3.954-961.1992]

[26] Jin WJ, Kim B, Kim D, Choo HYP, Kim HH, et al. NF-κB signaling regulates cell-autonomous regulation of CXCL10 in breast cancer 4T1 cells. Exp Mol Med 2017;49:e295. [PMID: 28209986 DOI: 10.1038/emm.2016.148]

[27] Hsieh CC, Wang CH, Huang YS. Lunasin attenuates obesity-associated metastasis of 4T1 breast cancer cell through anti-inflammatory property. Int J Mol Sci 2016;17:2109. [PMID: 27983683 DOI: 10.3390/ijms17122109]